Adsorption Site Preference Determined by Triangular Topology: Application of the Method of Moments to Transition Metal Surfaces

Tsuji, Yuta
Faculty of Engineering Sciences, Kyushu University

Yoshizawa, Kazunari
Institute for Materials Chemistry and Engineering, Kyushu University

出版情報：The Journal of Physical Chemistry C. 126 (31), pp.13505-13519, 2022-08-11. American Chemical Society
バージョン：

Adsorption Site Preference Determined by Triangular Topology: Application of the Method of Moments to Transition Metal Surfaces

Yuta Tsuji,[1*] Kazunari Yoshizawa[2]

1. Faculty of Engineering Sciences, Kyushu University, Kasuga, Fukuoka 816-8580, Japan

2. Institute for Materials Chemistry and Engineering, Kyushu University, Nishi-ku, Fukuoka 819-0395, Japan

* To whom correspondence should be addressed.
E-mail: tsuji.yuta.955@m.kyushu-u.ac.jp

Abstract: The adsorption sites of top and hollow on the close-packed surfaces of transition metals are well known. In this paper, which site is more preferred for the adsorption of atoms and molecular fragments on the metal surfaces is discussed based on the topology of the adsorption geometry. For this purpose, the method of moments for the electronic density of states is applied to the surface. Adsorption at the hollow site generates triangular topology, leading to a more negative value of the third moment (μ_3) than that at the top site, which generates no triangular topology. When the difference in energy between the two adsorption sites is plotted against the band filling of the metal surface, a characteristic node at around the intermediate band filling can be found. This is a signature that the energy difference curve is controlled by μ_3. Roughly speaking, the hollow site adsorption, which has a more negative μ_3 value, takes precedence at low band fillings, while the top site adsorption, which has a less negative μ_3 value, takes precedence at high band fillings. One can conclude that an adsorption structure with more three-membered rings on a surface is more stable at low electron counts whereas that with less three-membered rings is more stable at high electron counts. However, if the strength of the metal-adsorbate bond is significantly greater than that of the metal-metal bond, the effect of the second moment (μ_2) on the energy difference curve cannot be neglected. The hollow-site adsorption leads to a larger value of μ_2 due to the topological feature of a larger coordination number around the adsorbate atom. As a result, the hollow site adsorption is preferred over the top site at any band fillings.

1. Introduction

The adsorption of atoms, molecules, and molecular fragments on transition metal surfaces plays an important role in various fields, such as catalysis,[1,2,3] adhesion,[4] corrosion,[5] friction,[6] and molecular electronics[7,8,9] among others. Especially in the field of catalysis, the importance of adsorption interactions on transition metal surfaces has long been recognized.[10,11] Many researchers have worked on the measurement and estimation of adsorption energy (heat of adsorption).[11,12,13,14,15] In addition to the energetics of adsorption, knowledge of the geometry of the interface between a metal surface and an adsorbate is very important in considering the catalytic and other effects of the surface. Infrared absorption spectroscopy has provided a basic insight into the adsorption structure.[16,17,18] More complex adsorption structures can be deduced on the basis of measurements using low-energy electron diffraction[19,20,21] and high-resolution electron-energy-loss spectroscopy.[22,23,24,25,26] Diverse adsorption structures observed with various methods, as exemplified above, are thoroughly compiled in a book by Somorjai and Li.[27]

Many theoreticians have discussed the energy difference between distinct adsorption sites of adsorbed species on the background of the availability of density functional theory (DFT) calculations for surfaces with the advancement of computational power and methods. For example, Vasić et al.[28] computationally approached the adsorption structure and energy of a hydrogen atom on transition metal surfaces; Kristinsdóttir and Skúlason[29] constructed the

potential energy surfaces for H adsorption on the close-packed surfaces of almost all the transition metals; Bernard Rodríguez and Santana[30] calculated the energies of a sulfur atom adsorbed at different adsorption sites on low index surfaces of several transition metals; Li and co-workers[31] computationally investigated the variation in adsorption geometry of NO on transition metal (111) surfaces. They found that the preference for each adsorption site is different for each metal. Interestingly, even for the same metal surface, there is also a theoretical study reporting the preference of adsorption sites varies with surface charge.[32]

To understand which adsorption structure is most stable on a metal surface, one may have recourse to the analysis of orbital interactions between the surface and the adsorbate.[33,34] Using theoretical techniques, such as Crystal Orbital Overlap Population (COOP), Crystal Orbital Hamilton Population (COHP), and Fragment Molecular Orbital (FMO) analyses, in conjunction with extended Hückel and/or DFT calculations, Hoffmann and co-workers have rationalized the stable adsorption structures of various adsorbed species on metal surfaces from the point of view of orbital interactions,[35,36,37,38] but it seems to be mostly a matter of molecules or molecular fragments adsorbed on the surface. For example, CH, CH_2, and CH_3 essentially have different orbitals that interact with surface orbitals,[36] and thus prefer different adsorption sites.

It would be of significant help to view the adsorption of atoms, molecules, and molecular fragments on metal surfaces by analogy with the interaction between the central

metal cation and the ligand in a metal complex.[35] There is a concept that characterizes ligands, which may be useful in this study: if two ligands have a very similar electronic description (the same number of frontier orbitals, the same symmetry properties, the same occupation by electrons, and among others), they can be said to be in the relationship of the isolobal analogy.[33,39,40] As mentioned in the previous paragraph, if the adsorption structure depends heavily on the properties of the adsorbed molecule or fragment itself, why not try to remove the dependence by using the isolobal analogy?

In this study, we mainly address the issue of the selectivity of adsorption sites on transition metal surfaces for ligands that are in the isolobal relationship. Figure 1 shows a simple way to see how the isolobal relationship links various main group fragments.[33] The upper row of this figure includes a dihydrogen molecule plus hydrides of non-metallic main group elements of the second period. In the lower row, the fragments obtained by removing one hydrogen atom from them are shown. The fragments thus generated have a single frontier orbital with one electron in it which participates in interfragment bonding.[41]

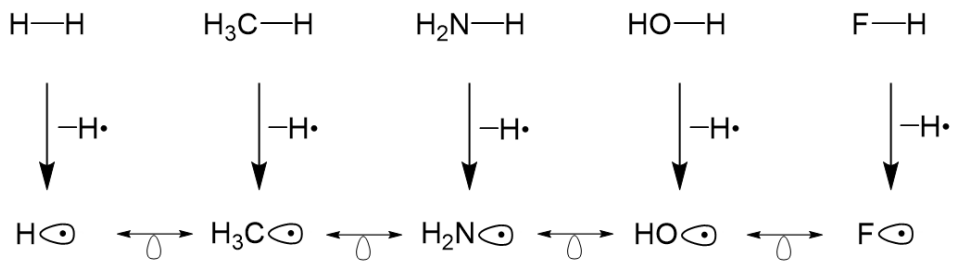

Figure 1. Generation of the isolobal relationship between main group fragments.

When the ligands shown in the bottom of Figure 1 are adsorbed on transition metal surfaces, which adsorption site is preferred? Based on the isolobal analogy, the selectivity of the adsorption sites of these ligands can be attributed to the nature of the metal itself that constitutes the surface. In addressing this issue, it would be reasonable to start with the close-packed (low-index) surface because such surfaces are stable and have been widely used as models of transition metal surfaces.[42,43,44,45] The close-packed surface structure reflects the bulk crystal structure of each metal. Figure 2a summarizes whether each of the third (5d) series of transition metals crystallizes in the body-centered cubic (bcc), face-centered cubic (fcc), or hexagonal close-packed (hcp) lattice. In Figure 2b through 2d, Ta, Re, and Ir are chosen as representatives of the bcc, hcp, and fcc metals, respectively, to visualize the structures of their close-packed surfaces: bcc (110), hcp (0001), and fcc (111) surfaces. In this figure, three typical adsorption sites of top, bridge, and hollow are indicated.

There are actually two types of hollow sites: fcc hollow sites and hcp hollow sites. The adsorption site we call H in Figures 2c and 2d is the fcc hollow site. Since it is known that the adsorption at the fcc site is more stable than that at the hcp site in many adsorption systems,[46,47,48,49] we will limit our discussion on the adsorption at the hollow to the fcc one below.

(a)

La	Hf	Ta	W	Re	Os	Ir	Pt	Au
hcp	hcp	bcc	bcc	hcp	hcp	fcc	fcc	fcc

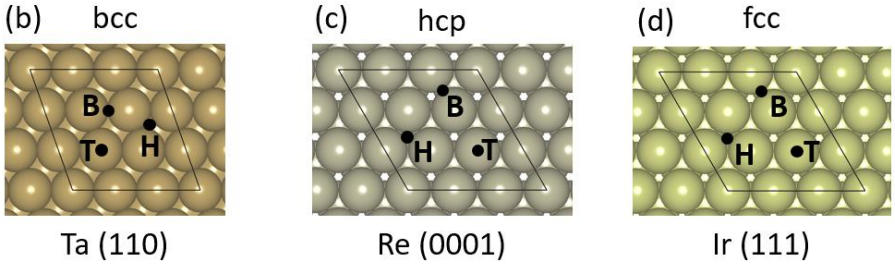

Figure 2. (a) List of the third (5d) series of transition elements: whether they belong to the bcc, hcp, or fcc family is shown. The close-packed 3 × 3 surfaces of (b) bcc(110), (c) hcp(0001), and (d) fcc(111) are shown: Ta, Re, and Ir are chosen as representatives of the crystal systems of bcc, hcp, and fcc, respectively. The typical adsorption sites of top (T), bridge (B), and hollow (H) are indicated by black dots.

In this paper, we will try to rationalize which adsorption sites are preferred when the ligands shown in the bottom of Figure 1 are adsorbed on the surface of each transition metal shown in Figure 2. It must be mentioned that there is a thorough previous study by Hoffmann and co-workers.[35,36,37] They have estimated the energy difference between each adsorption structure with the extended Hückel method and/or DFT method. The energy difference has been rationalized quite nicely based on the interaction between the surface orbitals and the fragment orbitals. From the energy values they calculated, we can learn that the ligands shown in Figure 1 do not prefer to be adsorbed at the bridge site by and large. Therefore, in this paper, the discussion will mainly focus on the difference in the stability of adsorption at the top and hollow sites.

What is the point of revisiting the subject, which has already undergone a thorough

examination by Hoffmann and co-workers? In the present study, we actually calculate the orbitals for the adsorbed structures, but we will mainly focus on something different from the orbital, linking geometry and energy: the method of moments originally proposed by Cyrot-Lackmann and co-workers.[50,51] We will detail the topological aspects of adsorption, grounded in orbital interactions at the interface between the surface and the adsorbate.

To establish the relationship between geometric structures and electronic states in various solids, Burdett and Lee developed the method of moments within the framework of the simple Hückel method, in which the atomic orbital basis set is considered orthogonal when the Hamiltonian is diagonalized, for which the formulas are significantly simpler.[52,53,54,55,56,57] The method of moments has been applied not only to the solid phase but also to metal clusters[58,59] and two-dimensional lattices.[60] Recently, Fredrickson and co-workers have attempted to extend the concepts of chemical pressure and acid-base in various intermetallic compounds based on the method of moments.[61,62,63,64]

We use the method of moments to tackle the problem of selectivity of adsorption sites. We are not the first to try to use the method of moments for surface problems. Cyrot-Lackmann actually used the method of moments to get a good estimate of the surface tension of transition metals as early as 1969.[65] The method of moments has been used by many researchers to calculate the electronic structures of various surfaces.[66,67,68,69] However, to the best of our knowledge, the method of moments has never been applied to the problem of adsorption on

surfaces. Therefore, our approach, detailed below, would be more or less novel.

The composition of this paper is as follows. First, in Section 2, Theoretical Background, we show how to link geometric structures and electronic states using the method of moments. Since many reviews and accounts[52,53,54,56,57] have been written on this subject, we will give a brief explanation to the extent that it does not compromise the self-contained nature of this paper. Then, in Section 3., Computational Methods, we describe the setup of our DFT calculations for the surface, and in Section 4, Results and Discussion, we present how to analyze and understand the results. Finally, in Section 5, Conclusions, we state our conclusions.

2. Theoretical Background

Mathematically, the *n*th moment (μ_n) is defined as the trace of the Hamiltonian matrix (**H**) to the *n*th power:[52,53,54,60,62,63]

$$\mu_n = \mathrm{Trace}\mathbf{H}^n = \sum_{i_1}\sum_{i_2}\cdots\sum_{i_n} H_{i_1 i_2} H_{i_2 i_3}\cdots H_{i_n i_1} = \sum_k E_k^n, \quad (1)$$

where μ_n can also be expressed as the sum of products of Hamiltonian matrix elements (H_{ij}) as well as the summation over all the eigenvalues (E_k) to the *n*th power. As is clear from the last equivalence in eq. 1, the *n*th moment for extended systems, whose electronic structure is described by the density of states (DOS), is defined as[52,62]

$$\mu_n = \int_{-\infty}^{\infty} E^n \mathrm{DOS}(E)\, \mathrm{d}E. \quad (2)$$

As indicated by the second equivalence in eq. 1, in terms of the geometric structure or topology

of the structure, the *n*th moment can be interpreted as the weighted sum over all closed walks of length *n* amongst all the orbitals of the system.

Figure 3 shows the adsorption structure of an adsorbate at the top and hollow sites. Their structures are truncated to the smallest units and the topology of the resulting structures is represented as G_1 and G_2. The adjacency matrices describing G_1 and G_2 are respectively expressed as

$$\mathbf{A}(G_1) = \begin{bmatrix} 0 & 1 & 0 & 0 \\ 1 & 0 & 1 & 1 \\ 0 & 1 & 0 & 1 \\ 0 & 1 & 1 & 0 \end{bmatrix}, \tag{3}$$

and

$$\mathbf{A}(G_2) = \begin{bmatrix} 0 & 1 & 1 & 1 \\ 1 & 0 & 1 & 1 \\ 1 & 1 & 0 & 1 \\ 1 & 1 & 1 & 0 \end{bmatrix}. \tag{4}$$

Here we have used the rudiments of chemical graph theory.[70,71,72]

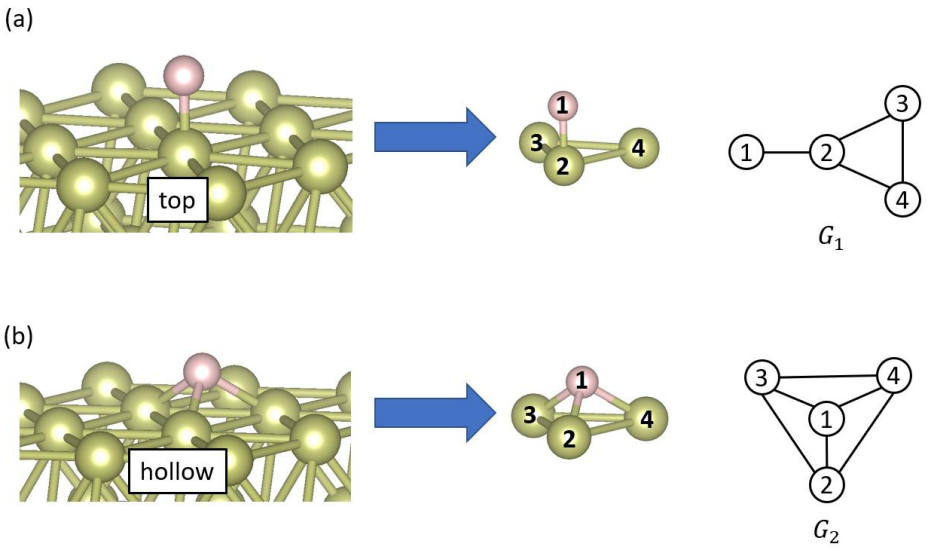

Figure 3. Adsorption structures of an adsorbate at the (a) top and (b) hollow sites (left). These structures are truncated to the smallest unit and its topology is represented by a graph (right).

Let us consider the adjacency matrices of eqs. 3 and 4 as Hückel matrices to obtain the eigenvalue spectrum. In chemical graph theory, one typically states that $\mathbf{H} = -\mathbf{A}$.[71] The eigenvalue spectrum obtained by just diagonalizing the Hamiltonian thus obtained is shown in Figure 4a. Within the framework of the Hückel method, the total electronic energy of the system amounts to[73]

$$E_{\mathrm{tot}}(N) = \sum_k n_k E_k, \tag{5}$$

where n_k is the occupation number of the kth orbital so that $\sum_k n_k = N$. Using eq. 5, one may plot the total electron energy of the system as a function of the number of electrons. Also, the energy difference between two systems may be plotted as a function of the number of electrons. However, if we use the eigenvalues obtained by just diagonalizing the Hamiltonian as the orbital energy in eq. 5, we may get wrong results. One has to use the set of eigenvalues obtained via the procedure called second moment scaling:[53,54,55,56,57] The relative energy within the Hückel formalism has to be evaluated from calculations where the second moments are set equal.

That one needs to do such an operation can be traced back to the fact that the Hückel Hamiltonian does not contain repulsive interactions[57] and to avoid this problem one relies on the structural energy difference theorem.[74] Note that since $\mu_2 = \sum H_{ij}H_{ji}$, one view of μ_2 is a measure of the coordination strength around an atom. The repulsive energy depends only on nearest atomic neighbors and so it should be proportional to μ_2.[56] Without second moment

scaling, the structure with the highest coordination number is usually calculated to be the most stable.[53]

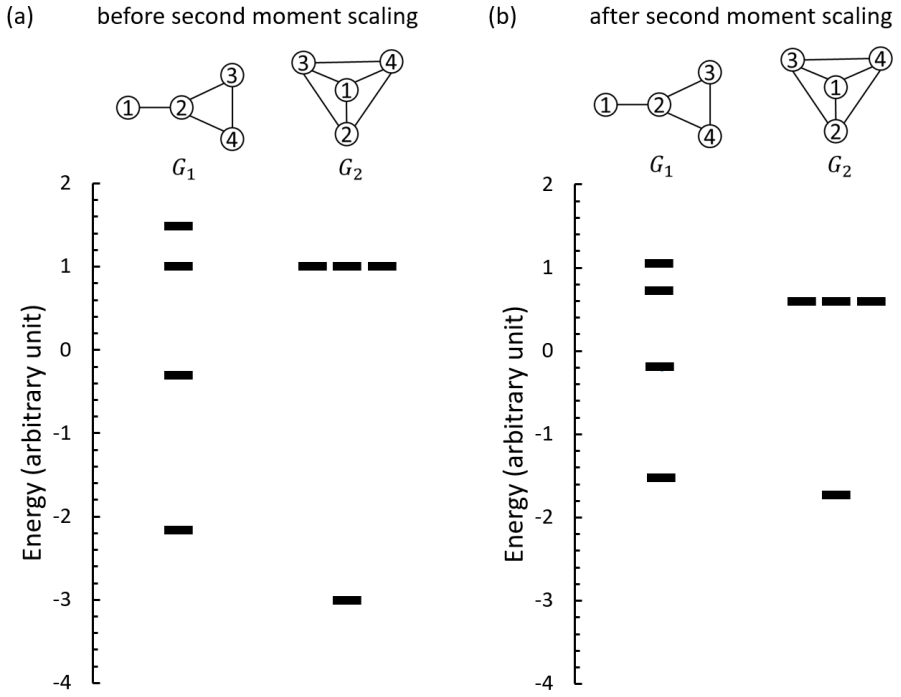

Figure 4. Eigenspectra for graphs G_1 and G_2 (a) before and (b) after second moment scaling.

The eigenvalue spectrum after applying second moment scaling to the eigenvalue spectrum shown in Figure 4a is shown in Figure 4b (see the literature[75] for how to do second moment scaling). Here the energy spectrum is scaled so that $\mu_1/\mu_0 = 0$ and $\mu_2/\mu_0 = 1$. By applying eq. 5 to the eigenvalue spectrum shown in Figure 4b, it is possible to plot the energy difference between the structures represented by graphs G_1 and G_2 as a function of the number of electrons (see Figure 5). The oscillatory trends in structural stability can be directly related to the topology of the molecule by the moments theorem first introduced by Ducastelle and Cyrot-Lackmann

in 1971.[51]

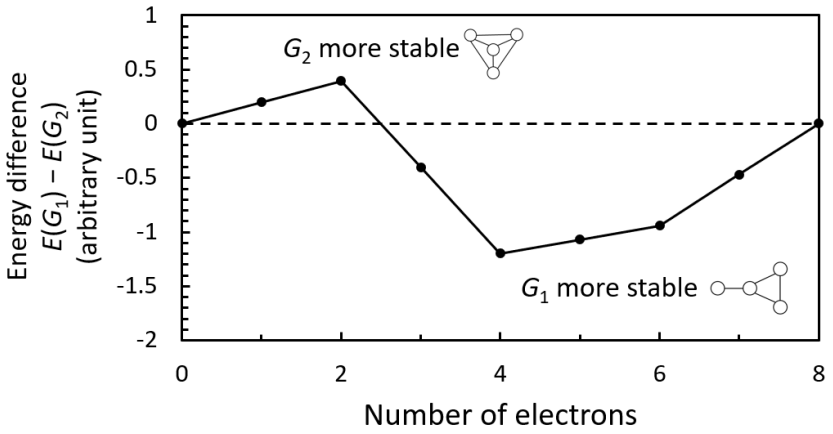

Figure 5. Plot of the energy difference between the structures represented by graphs G_1 and G_2 as a function of the number of electrons. For the generation of this plot, the energy spectra shown in Figure 4b were used. A positive value means that the structure represented by G_2 is more stable whereas a negative value means that the one by G_1 is more stable.

One important feature observed in Figure 5 is that the number of nodes in the energy difference curve (including those at $N = 0$ and 8) is 3, which is equal to the order of the first disparate moment between the two.[53] Owing to second moment scaling, both have the common moment at least up to the second order. The values of μ_3/μ_0 evaluated for G_1 and G_2 are -0.53 and -1.15, respectively. The energy difference curve here is of the form expected for a third moment problem. Another important feature associated with this energy difference curve is that it is the structure with the more negative third moment value which is the one that is more stable at the earliest orbital occupancy.

There are contributions to μ_n from the closed walks of length n that connect orbitals

with non-zero values of H_{ij}. Since the orbital walks that are possible are determined by the atomic connectivity, one can link μ_n to the topology of the atomic network via the orbital connectivity.[52,53,54] The fact that the value of μ_3 evaluated for G_2 is more negative than that for G_1 clearly corresponds to the topological feature that G_2 contains more triangles in its structure than G_1.

The most important thing we can learn from Figure 5 is that the structure with more three-membered rings is more stable at low electron counts whereas the structure with less three-membered rings is more stable at high electron counts. The stability of the two is close at too high, too low, or middle electron counts. This can be proven mathematically and is shown in the literature along with more general statements.[56] We discuss adsorption based on this concept. Based on Figure 5, we may say that adsorption to the hollow site is preferred on early transition metal surfaces, while that to the top site is preferred on late transition metal surfaces.

In Figure 3, we have truncated the close-packed surface of the transition metal to the limit so that it can be represented by a triangle with three metal atoms. The resultant cluster model for the surface seems extremely small and oversimplified; we may as well consider a larger cluster model with more remaining surface features. Based on this idea, the models shown in Figure 6a were generated. In the same way that we obtained the energy difference curve shown in Figure 5, we calculated it for these models, and the results are shown in Figure 6b. Since these models consist of eight sites, eight energy levels are produced. Thus, they can

accept up to 16 electrons, so the range of the horizontal axis in Figure 6b is from 0 to 16.

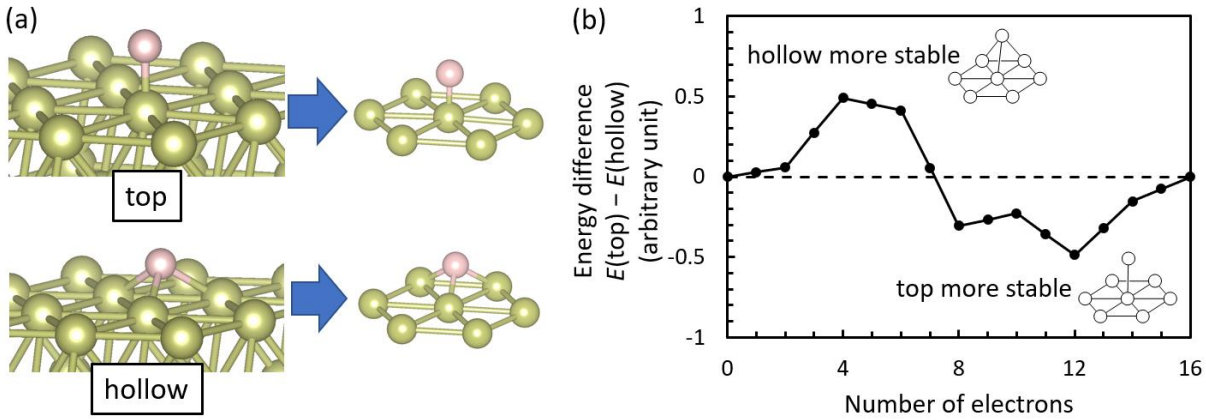

Figure 6. (a) Adsorbed structures of an adsorbate at the top and hollow sites are truncated to a moderately sized fragment model for graph representation. (b) The energy difference curve calculated for the graphs obtained in (a), plotted against the number of electrons. A positive value means that the adsorption structure at the hollow site is more stable whereas a negative value means that the one at the top site is more stable.

There are three nodes in the energy difference curve shown in Figure 6b, which has the appearance expected for the third moment problem. The topology corresponding to the hollow-site adsorption is more stable in the region with a small number of electrons and its value of μ_3/μ_0 is evaluated to be -0.93, whereas that corresponding to the top-site adsorption is more stable in the region with a large number of electrons and its value of μ_3/μ_0 is evaluated to be -0.77. The structure with the more negative μ_3 value is more stable at low electron counts. It can be seen that the difference in the number of triangles in the structure affects μ_3, which in turn creates the difference in stability depending on electron counts. In these respects, Figure 5 and Figure 6b are essentially similar. Of course, one looks at the details, finding a number of

differences; however, it would be allowed to say that the graphs G_1 and G_2 shown in Figure 3 are the minimal models to show the essential differences characteristic of these systems.

It should be noted that a lot of details have been lost when we moved from the actual surface adsorption structure to the chemical graphical representation, as shown in Figure 3. Here, it would be informative to organize the specifics that have not been retained through the abstraction. 1) It is assumed that the strength of the metal-metal (M-M) bond and that of the metal-adsorbate (M-Ad) bond are equivalent. 2) The basis orbitals involved in such bonds are assumed to be isotropic with one orbital per atom. 3) These orbitals are assumed to be orthogonal and their energy levels are assumed to be the same even for different elements. Thus, it seems that our model is oversimplified. Below, let us examine the results of first-principles calculations to see if the model captures the essence of adsorption.

3. Computational Methods

We performed first-principles calculations of adsorption using a slab model. The top view of the surface model we used has already been shown in the bottom of Figure 2. The close-packed 3 × 3 surfaces of (110), (0001), and (111) were chosen for the bcc, hcp, and fcc metals, respectively. The slab consists of three atomic layers, and the bottom two layers were fixed during the geometry optimization. A vacuum layer with a thickness of more than 10 Å was added in the vertical direction of the surface.

The structures of H, CH_3, NH_2, OH, and F adsorbed at a hollow or top site on the surfaces of La, Hf, Ta, W, Re, Os, Ir, Pt, and Au were optimized with periodic boundary DFT, as implemented in Vienna ab initio simulation package (VASP) 5.4.4.[76,77,78,79] For comparison, the adsorption of N and O were also computed. Some readers may be interested in the adsorption sites of alkanethiol (or alkanethiolate). This is because its interface with metal surfaces is very important in organic electronic devices.[38, 80 , 81] We have additionally investigated the adsorption sites of methyl thiolate (CH_3S). The generalized gradient approximation was adopted with the functional described by Perdew, Burke, and Ernzerhof.[82] The Kohn–Sham equations were solved with a plane-wave basis set using the projector-augmented wave method.[83,84] The cutoff energy for the plane-wave basis set was set to 500 eV. The convergence threshold for self-consistent field iteration was set to 1.0×10^{-5} eV. The structure was relaxed until the forces on all of the atoms are less than 0.05 eV/Å. The Γ-centered k-point meshes with k spacing of $2\pi \times 0.05$ $Å^{-1}$ were employed for sampling the Brillouin zone. Grimme's D3 dispersion correction formalism with Becke-Johnson damping[85] was adopted. We have confirmed in our previous study that this is a good method for adequately describing atomic interactions at surfaces.[86] Surface structures shown in this paper were drawn by using VESTA.[87] To estimate the strength of the bonding of the adsorbates to the surface, we calculated the integrated COHP (ICOHP)[88,89,90] using LOBSTER v4.0.0.[90,91,92] The ICOHP is known to be a good measure of covalent bond strength.[1,4,93,94] LOBSTER was also used to

perform the Mulliken population analysis.

We performed extended Hückel calculations[95] to understand the results of the DFT calculations in connection with the simple models presented in the Theoretical Background section, using ATK-SE[96] implemented in QuantumATK[97] and YAeHMOP[98] implemented in Avogadro.[99] The standard atomic parameters taken from the literature[100] were adopted.

4. Results and Discussion

The energy difference curves for the two adsorption modes, top and hollow, of the five types of adsorbates, H, CH_3, NH_2, OH, and F, on the transition metal surfaces calculated with DFT are shown in Figure 7 as a function of valence electron count. The optimized structure for each adsorbed species on each surface is shown in the Supporting Information (SI) to this paper. Almost all adsorbed species were successfully optimized at both adsorption sites. However, in some cases, the adsorption structure at an adsorption site was not found to be a local minimum. In such a case, we performed a partial optimization of the adsorption structure by fixing the *x* and *y* coordinates but relaxing the *z* coordinate of the atom closest to the surface in the adsorbed species. The information about which structures the partial optimization was performed on is presented in the SI.

Compare the shape of the computed curves in Figure 7 with that in Figure 5. Notice that adsorption to the hollow site is more preferred at low electron counts while that to the top

at high electron counts. The reversal of preference for the adsorption site occurs around W to Os. As such, the preference for the adsorption site is clearly a third moment problem.

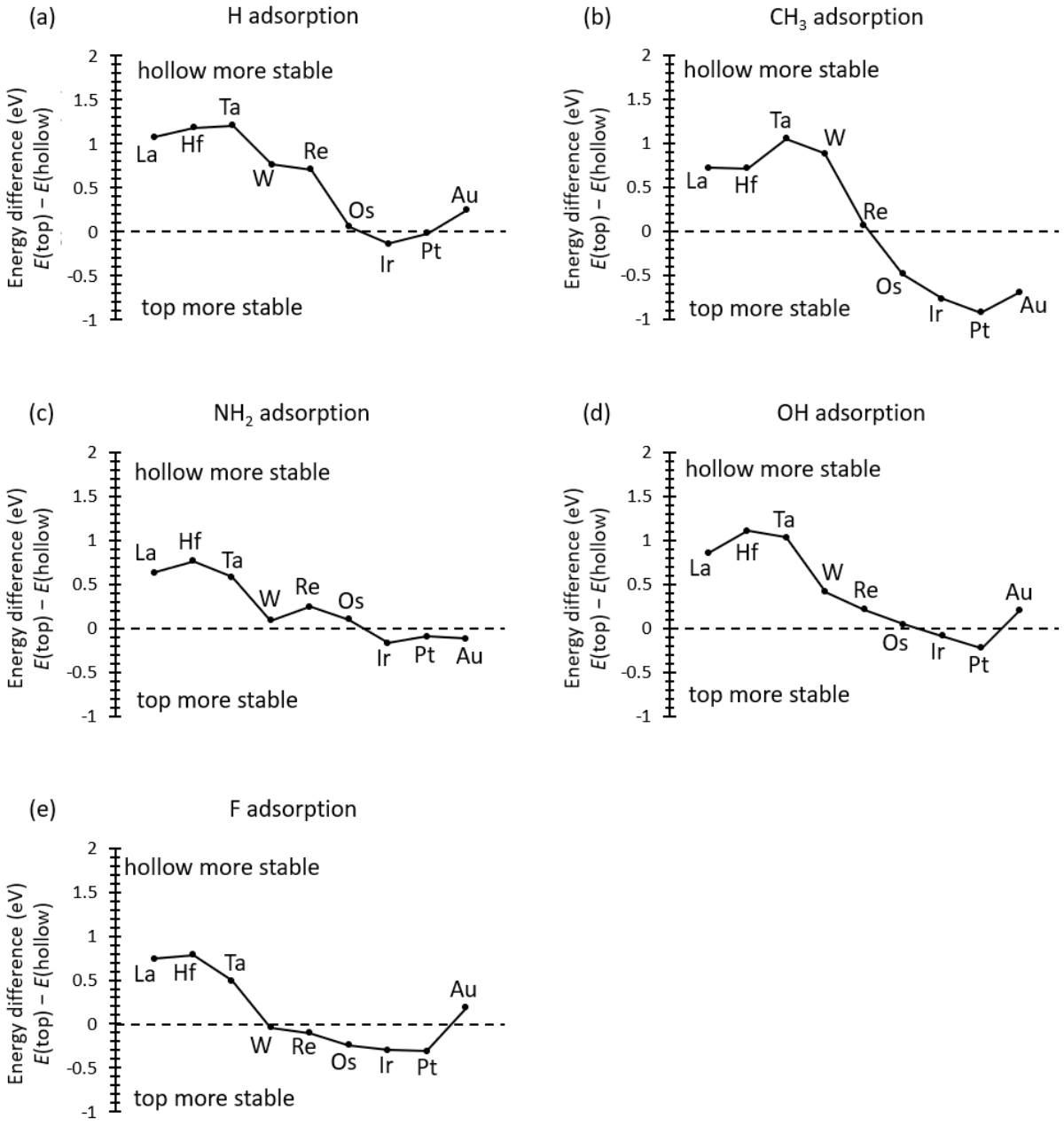

Figure 7. Energy difference curves for the adsorption structures at the top and hollow sites on the close-packed 5d transition metal surfaces computed for the adsorbates of (a) H, (b) CH_3, (c) NH_2, (d) OH, and (e) F. When the value is positive, the adsorption at the hollow site is more stable.

We have drawn these curves using the calculation results for the adsorbates that are isolobal with each other, but there seems to be more or less influence by the type of adsorbate. For CH_3 adsorption, there is a clear distinction between the preference for the top and hollow sites. In other words, the peak amplitude of the curve is large. On the other hand, the amplitudes of the curves for the other adsorbed species are small. In particular, in the adsorption of H, the overall preference for the hollow site appears to be more pronounced. This is the opposite of the trend seen in Figure 5, where the preference for the top site is rather pronounced.

Let us look at the results for the adsorption of N and O atoms, which were calculated for comparison (see Figure 8). The stability of the hollow site increases from La to Hf, followed by a decrease in the stability from Hf to Re or Os, and again an increase in the stability from Re or Os to Pt or Au. In that at low band fillings, the stability of adsorption at the hollow site is remarkable, but as the bands are filled with electrons, the predominance of adsorption at the hollow site declines, hitting bottom somewhere at high band fillings, the curves in Figures 7 and 8 share similarities. In Figure 8, however, the stability of adsorption at the top site does not outweigh that at the hollow site at any electron counts. Nevertheless, based on the general shape of the curves, we may say that the third moment plays some role in the adsorption of these atoms as well. A similar trend was observed in the adsorption of alkanethiol (see the SI).

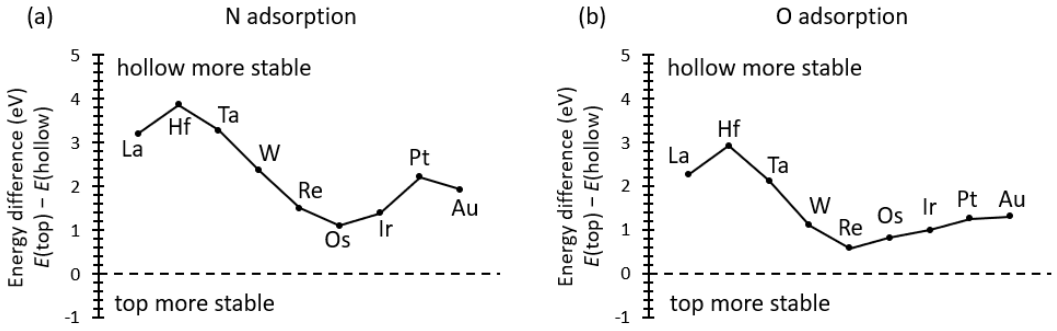

Figure 8. Energy difference curves for the adsorption structures at the top and hollow sites on the close-packed 5d transition metal surfaces computed for the adsorbates of (a) N and (b) O. When the value is positive, the adsorption at the hollow site is more stable.

It is very interesting to note that these curves are very similar to that obtained using the very simple model. Our model dose not miss the essence in the adsorption of atoms and molecular fragments on the transition metal surfaces. However, there still seems to be a large gap between our simple models (Figures 5 and 6) and the transition metal surfaces on which an atom or a molecular fragment is adsorbed. In the following, we show the results of our efforts to close the gap. For this purpose, we have used the extended Hückel calculation, which is probably the best method that can mediate between the simple Hückel model and the DFT computations.

In Figure 6, we can see that the third moment is clearly dominant in the energy difference curve for CH_3 adsorption, so we decided to perform extended Hückel calculations for it. For the sake of simplicity, we could have investigated hydrogen adsorption. However, we dared to face the complexity.

In the block of the periodic table we are interested in, Re is right in the middle. So let

us start to consider the structure of CH_3 adsorbed at the top or hollow site on the Re(0001) surface optimized with DFT. It would be interesting to consider calculating an energy difference curve with the Re surface set to different charges at the extended Hückel level. By calculating a state where all Re atoms in the unit cell have a charge of +1, we may be able to calculate a pseudo W surface. Since our unit cell contains 27 metal atoms, it yields a huge charge of +27. The calculation of such a system with a large charge is unlikely to converge when the normal DFT method is applied, but this is not a problem with the extended Hückel method because the parameters are independent of the charge.[101] Our approach, which assumes that only the number of electrons and the position of the Fermi level change while the band structure and density of states remain unchanged, is in the spirit of the rigid-band model.[102] In this way, we obtained the energy difference curve as shown in Figure 9.

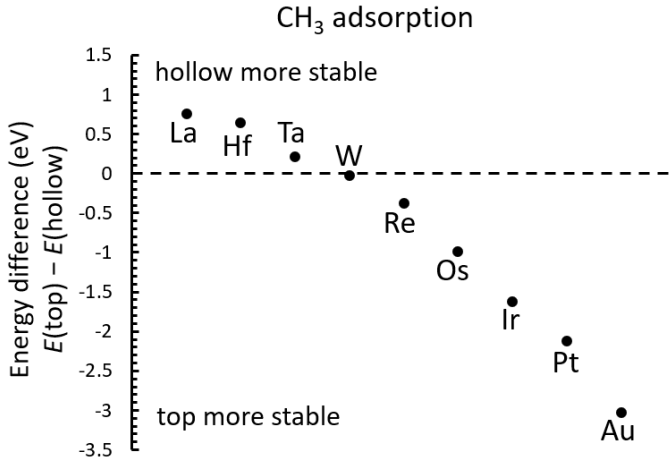

Figure 9. Energy difference curve for CH_3 adsorption calculated at the extended Hückel level. DFT-optimized structures of CH_3 on the Re(0001) surface were used. By varying the number of electrons in the unit cell while keeping the band structure and the shape of the density of states fixed, the energy difference for the other metal surfaces was calculated.

As the metal element changes, the number of valence electrons, crystal structure, metal-to-metal bond length, valence orbital level, and bond distance between the metal and the adsorbed species change. In our calculations to obtain Figure 9, all of these changes except for the change in valence electron counts were ignored. In addition, the essential difference between the DFT method and the extended Hückel method, namely the non-inclusion of the electron-electron interaction, must also be kept in mind.[103] Nevertheless, this calculation qualitatively reproduces the most important trend suggested in Figure 7, which is the preference for adsorption to the hollow site when the band filling is low and to the top site when the band filling is high. Therefore, the effects of different band occupancies on the energy difference are considered to be critical for the selectivity of the adsorption sites.

What is included in the calculation to obtain the energy difference curve shown in Figure 9, but not included in the calculations to obtain those shown in Figures 5 and 6? It is the directivity of the basis functions. Nevertheless, in the simple model, the metal atoms and adsorbate are not treated only as single s orbitals. For example, the three types of orbital interactions shown in Figure 10a, are all described by the adjacency matrix shown in Figure 10b. Even for systems with more complicated orbital interactions where d_{xz} and d_{yz} orbitals are involved in the π conjugation, the topology and electronic structure can be described within the framework of the simple Hückel method.[73]

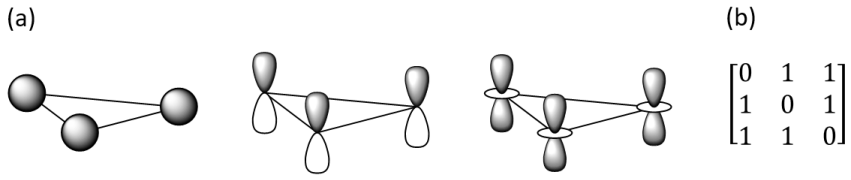

Figure 10. (a) Triangular orbital interactions formed by three s, p_z, and d_{z2} orbitals and (b) the adjacency matrix to express their topology.

By clarifying the orbital interaction between the adsorbed species and the surface metal atoms, we will see whether the Hamiltonian matrix for the simple model is adequate to describe adsorption. For this purpose, we will discuss the results of the COOP analysis on the orbital interaction between the surface and the adsorbed species.

The COOP curves for the interactions between the carbon atom of CH_3 adsorbed at the top and hollow sites on the Re(0001) surface and the nearest Re atom (atoms) are shown in Figure 11. The position of the Fermi level of the Re surface is also shown in this figure. By reducing or increasing the number of electrons per unit cell of the slab model, the total number of electrons can be made the same as that of the La or Au surface, respectively. In this way, it is possible to estimate the Fermi levels of these surfaces, which are also shown. The Fermi level changes from about -14 to -8 eV as one moves from La to Au on the periodic table. Hence, one should pay particular attention to the COOP curve in that range. In interpreting the shift in the Fermi level, one should not make the mistake of thinking that because the Fermi level of Au appears to be located at the highest position, its work function would be the smallest. In fact,

the level of the d-orbitals goes down as one transitions from La to Au,[104] but that effect is not taken into account here. The height of the Fermi level of these surfaces is determined by the position and band occupancy of the d-bands.[34]

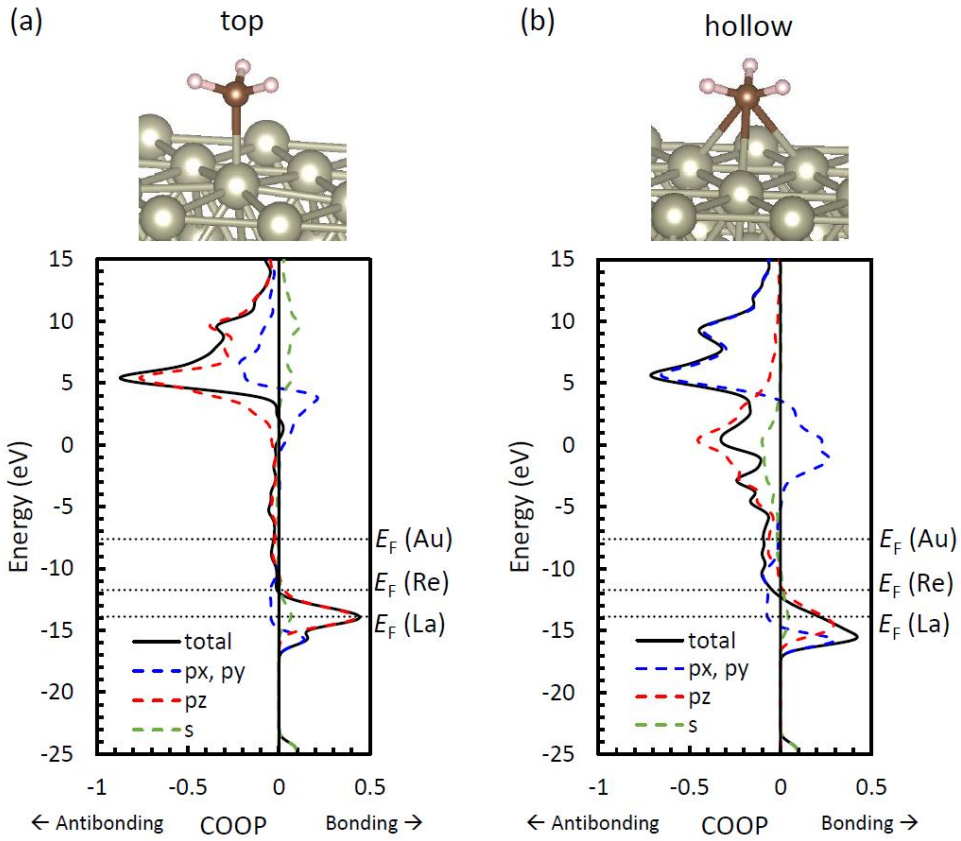

Figure 11. COOP curves calculated using the extended Hückel method for the Re-CH_3 bond (bonds) at the (a) top and (b) hollow sites on the Re(0001) surface. See the adsorption structure shown above each graph to get an idea of the structure around the Re-C bond (bonds) for which COOP was calculated. The total COOP curves (black solid line) for the Re-C bond (bonds) are partitioned into contributions from the $2p_x$ and $2p_y$ (blue dashed line), $2p_z$ (red dashed line), and 2s (green dashed line) orbitals of the carbon atom. The Fermi level of the Re surface is indicated by the black dotted line labeled E_F (Re). The Fermi level evaluated by reducing or increasing the band occupancy so that the total number of electrons in the unit cell is equal to that of the La or Au surface is indicated by the black dotted lines labeled E_F (La) or E_F (Au), respectively.

From Figure 11, one can see that the $2p_z$ orbital of the carbon atom is the main

contributor to the C-Re bond at the top site, while the contributions of the $2p_x$ and $2p_y$ orbitals are secondary. The picture is much the same when we move to the hollow site, but the importance of the $2p_x$ and $2p_y$ orbitals seems to have increased just slightly. Therefore, it is suggested that the σ-bond brought about by the $2p_z$ orbital of the carbon atom is more important than the π-bonds due to the $2p_x$ and $2p_y$ orbitals in the interaction between CH_3 and the transition metal surfaces. Assuming the isolobal analogy, this conclusion would also apply to the adsorption of H, NH_2, OH, and F.

Now that we have identified the adsorbate orbital involved in adsorption, let us try to identify the surface counterpart. That is obvious for adsorption at the top site. The $5d_{z2}$, 6s, and $6p_z$ orbitals have the proper symmetry to interact (see Figure 12a). The interaction of the dsp hybrid with the $2p_z$ orbital of the carbon atom has been detailed by Hoffmann and co-workers (see Figure 12b).[33,34,36] The topological aspect of the orbital interaction shown in Figure 12b may be described by the adjacency matrix in eq. 3.

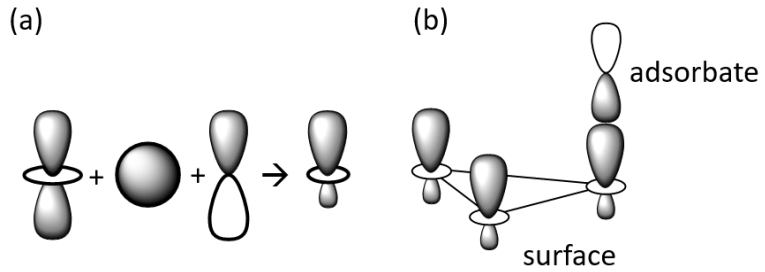

Figure 12. (a) Hybridization of d_{z2}, s, and p_z orbitals on transition metal surfaces that plays an essential role in their formation of a σ bond with an adsorbate. (b) Orbital interaction between the p_z orbital of the adsorbate and the three dsp hybrids of the transition metal surface.

The interaction between the $2p_z$ orbital of the C atom and the neighboring Re atoms is important for adsorption at the hollow site as well, as suggested in Figure 11b. To analyze it in more detail, we divided the interaction into contributions from the $5d_{z2}$, 6s, and $6p_z$ orbitals of the Re atoms and those from the $5d_{xz}$ and $5d_{yz}$ orbitals, as shown in Figure 13a. From this figure, it can be seen that the contribution of the dsp hybridization consisting of the $5d_{z2}$, 6s, and $6p_z$ orbitals seems still significant, but the contribution of the $5d_{xz}$ and $5d_{yz}$ orbitals may not be negligible. So it would be reasonable to understand the interaction based on the d^2sp hybridization shown in Figure 13b. As such, orbital interaction shown in Figure 13c can be assumed. Its topological aspect may still be described by the adjacency matrix in eq. 4.

In the literature, based on the isolobal analogy, it is pointed out that the orbital pattern of tetrahedral cluster compounds is topologically analogous to the hypothetical tetrahedral H_4 system.[33] Similar perspectives were provided by Hoffmann and co-workers in the analysis of orbital interactions between trinuclear complexes and ligands,[105] as well as those in the adsorption of ethylidyne at the hollow site on the surface of Pt(111).[106] What we have uncovered here is an extension of what has been uncovered in the previous studies.

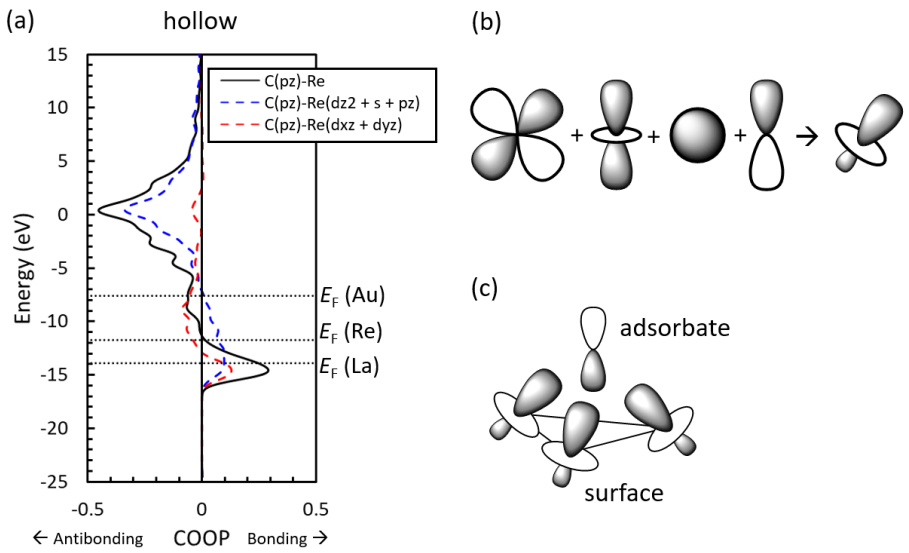

Figure 13. (a) COOP curve (black solid line) for the interaction of the $2p_z$ orbital of the C atom of CH_3 adsorbed at the hollow site of the Re(0001) surface with the neighboring Re atoms calculated at the extended Hückel level. This COOP curve is partitioned into contributions from the $5d_{z2}$, 6s, and $6p_z$ orbitals (blue dashed line) and the $5d_{xz}$ and $5d_{yz}$ orbitals (red dashed line) of the Re atoms. The Fermi level labels of E_F (Re), E_F (La), and E_F (Au) are the same as those shown in Figure 11. (b) Hybridization of d_{xz} (d_{yz}), d_{z2}, s, and p_z orbitals on transition metal surfaces that may play an essential role in their formation of a σ bond with the adsorbate is shown. (c) Orbital interaction between the p_z orbital of the adsorbate and the three d^2sp hybrids of the transition metal surface.

Can the orbital interactions and others typically depicted in Figures 12b and 13c be confirmed on the actual surfaces? Yes, we have carefully checked the wave functions (crystal orbitals) calculated at the Γ points for the slab models and mapped them to the wave functions derived from the simple, four-site models (see Figure 14). This figure suggests that the orbital interaction between the adsorbate and the surface can be described by the simple graph-theoretic model.

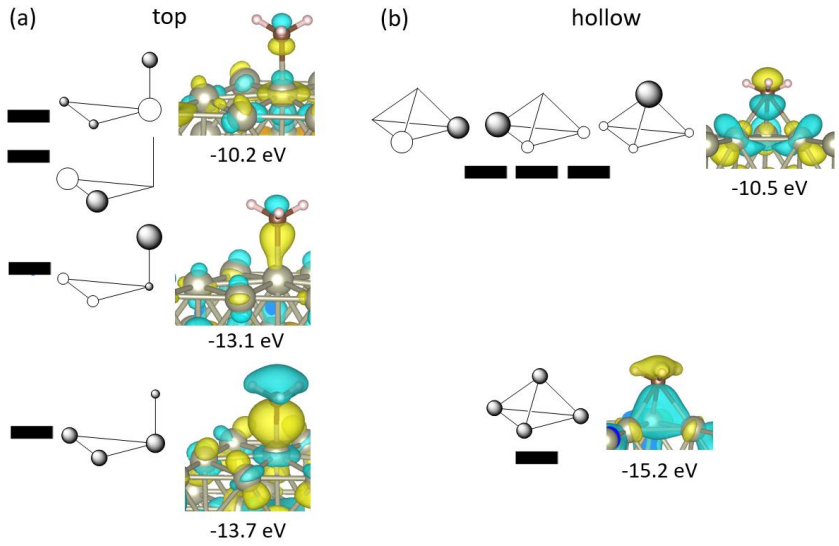

Figure 14. Correspondence between the wave functions for the simple models and those calculated for the slab models for the adsorption of CH_3 at the (a) top and (b) hollow sites. The wave functions for the slab models were calculated at the Γ point using the extended Hückel method. Their energies at the Γ point are also shown. The isosurface value is set to 0.03 $e^{1/2}/bohr^{3/2}$.

We have shown how to relate the simple model to the actual slab model for adsorption in terms of the topology of orbital patterns by focusing on orbital interactions. However, one more issue remains to be solved: how to relate the x-axis in Figure 5, i.e., the number of electrons, to that in Figures 7 and 8, i.e., the band filling. In the simple model, the band structure is filled at 2 electrons per atom, but things will be different for transition metal atoms with d electrons. Nevertheless, it is clear from the previous discussion that the d_{z2} orbitals of the surface and the p_z orbital of the adsorbate have the most important effect on the interaction between the surface and the adsorbate. We tackled the problem of correlating the x-axes by performing a population analysis of these orbitals.

We used LOBSTER to analyze the Mulliken gross orbital population for the orbitals

involved in the orbital interactions on the CH_3 adsorbed surfaces, based on the projection of the DFT-level wave functions output from VASP to local orbitals.[107,108] The results of these calculations are summarized in Tables 1 and 2. The population for the $2p_z$ orbital of the C atom fluctuates between 1.1 and 1.5, while that for the metal d_{z2} orbitals approaches 2 as one transitions from left to right in the periodic table. With the increase in the population of the metal orbitals, the sum of the populations also increases. In this calculation, the number of electrons per atom is at most 2, so the sum would be a good guide when getting an idea about the abscissa in Figure 5.

Table 1. Mulliken gross orbital population calculated for the $2p_z$ orbital of the C atom and $5d_{z2}$ orbitals of the transition metal atoms nearby in the structures of CH_3 adsorbed at the top site. The metal atom directly bonded to the carbon atom is denoted as M1. Although only information on the surface metal atoms near the C atom is shown, this calculation was performed using the slab model.

	La	Hf	Ta	W	Re	Os	Ir	Pt	Au
$2p_z$ (C)	1.34	1.49	1.38	1.38	1.35	1.35	1.25	1.11	1.21
$5d_{z2}$ (M1)	0.61	0.78	0.94	1.13	1.22	1.30	1.37	1.46	1.73
$5d_{z2}$ (M2)	0.29	0.53	0.75	0.90	1.12	1.30	1.55	1.86	1.96
$5d_{z2}$ (M3)	0.29	0.53	0.77	0.90	1.12	1.30	1.55	1.86	1.97
sum	2.53	3.33	3.84	4.31	4.81	5.25	5.72	6.29	6.87

Table 2. Mulliken gross orbital population calculated for the $2p_z$ orbital of the C atom and $5d_{z2}$ orbitals of the transition metal atoms nearby in the structures of CH_3 adsorbed at the hollow site. Although only information on the surface metal atoms near the C atom is shown, this calculation was performed using the slab model.

	La	Hf	Ta	W	Re	Os	Ir	Pt	Au
$2p_z$ (C)	1.38	1.48	1.40	1.41	1.37	1.42	1.32	1.18	1.21
$5d_{z2}$ (M1)	0.28	0.54	0.79	0.96	1.20	1.33	1.54	1.84	1.96
$5d_{z2}$ (M2)	0.27	0.54	0.78	0.94	1.20	1.32	1.54	1.84	1.95
$5d_{z2}$ (M3)	0.28	0.54	0.79	0.96	1.18	1.31	1.54	1.84	1.96
sum	2.21	3.10	3.76	4.27	4.95	5.38	5.94	6.70	7.08

In Figure 5, the preference for the adsorption sites is reversed when the number of electrons increases from 2 to 3. In Figure 7, on the other hand, it occurs around Re. From Tables 1 and 2, the total population evaluated for the Re surface is about 5. Therefore, there is a subtle difference that cannot be captured by the simple model calculation. So what are the details that our model fails to capture? We will go back to the Hückel calculation and clarify it by tweaking some parameters.

We shall start with the effect caused by the difference between the orbital levels of the adsorbate and the metal atom. Similar to the treatment of heteroatoms in the Hückel method,[73] we constructed Hamiltonian matrices as shown in Figure 15a. By varying the value of parameter α from 0, the difference in energy level between the adsorbed species and the transition metal atoms is taken into account. Electronegativity is useful in determining whether the value of α should be positive or negative.[33] There may be a lot of debate about how to define

electronegativity, but in general, adsorbed species consisting of main group elements are more electronegative than transition metal elements.[104,109,110,111] Therefore, α takes a negative value. The more electronegative the element of the adsorbed species, the more negative its value.

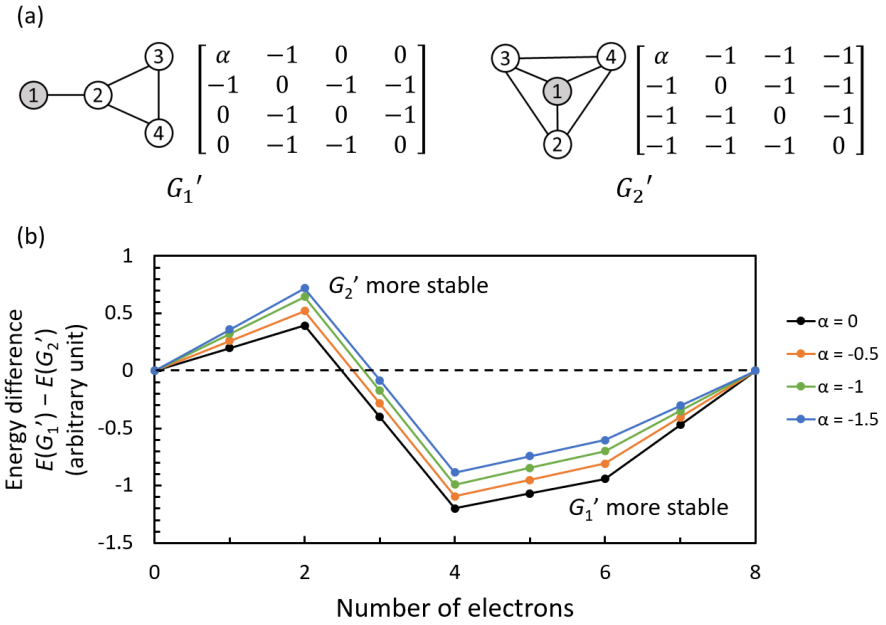

Figure 15. (a) Modified Hamiltonian matrices and corresponding graphs G_1' and G_2'. The shaded node corresponds to the adsorbate, whose energy level is represented by α with respect to the energy level of the metal atom. (b) The energy difference curve for G_1' and G_2' obtained by the method similar to that used to obtain the energy difference curve in Figure 5. Here, the value of α in the Hamiltonian matrices was varied from 0 to -1.5.

Figure 15b shows how the energy difference curve changes when α is set to a negative value and its absolute value is gradually increased. The depth of the valley bottom at high electron counts becomes shallower and shallower, while the height of the hill top at low electron counts becomes higher and higher. One can see how the region where adsorption at the hollow

site becomes stable is expanding. This change suggests that our ideal model is getting closer to reality.

Let us explore the cause of the change seen in Figure 15b. With the introduction of parameter α, walks of length 3 shown in Figure 16 have started to contribute to the third moment. It is clear from this figure that these walks appear to be counting the coordination number of the adsorbate atom. Since the coordination number is larger for adsorption at the hollow site, the number of walks contributing to μ_3 is also larger. As such, a more negative value of μ_3 for the hollow site adsorption ensues. This is how the stability of adsorption to the hollow at low band fillings is increased.

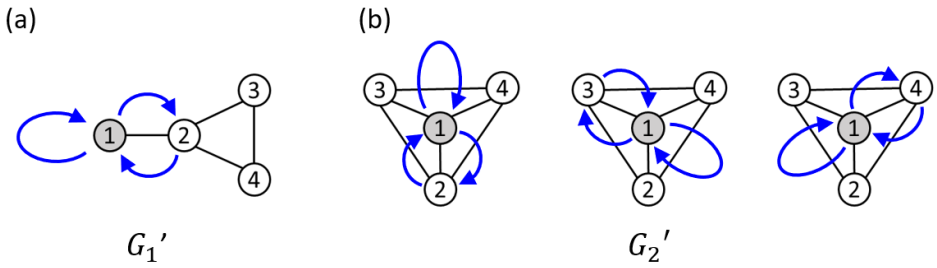

Figure 16. Walks on (a) G_1' and (b) G_2' (b) which get to contribute to the third moment due to the introduction of the parameter of α.

Since the level of the d-orbital of the transition metal decreases as one moves from left to right on the periodic table,[104] the difference between the energy level of the adsorbate and that of the metal atom shrinks. Thus, one may assume a model in which the absolute value of α becomes smaller as the number of electrons increases.

The next thing we will examine is the difference in coupling strength. In our model, all of the non-zero off-diagonal entries of the Hamiltonian matrix are set to the same value. This implies that the strength of the M-M bonds is assumed to be equivalent to that of the M-Ad bond. In general, however, this is not the case. Naturally, the strength of the bond will vary depending on the type of adsorbed species. Now, let us approach this problem by first examining the ICOHP for each bond.

For each metal, the ICOHP values per bond for the M-M bond in the bulk and the M-Ad bond at the surface were calculated, their averages shown in the SI. Based on the averages of the ICOHP, the ratio of the strength of the M-Ad bond to that of the M-M bond was calculated and plotted in Figure 17. Here are some of the features that are observed: 1) M-Ad bonds are generally stronger than M-M bonds, 2) the strength of M-Ad bonding at the top site is about two times greater than that at the hollow site, and 3) the ratio of bond strength tends to be larger at both ends. The last point is probably due to the fact that the M-M bond strength becomes weaker at both ends. This could be traced back to the cohesive energy tendency of each metal.[112]

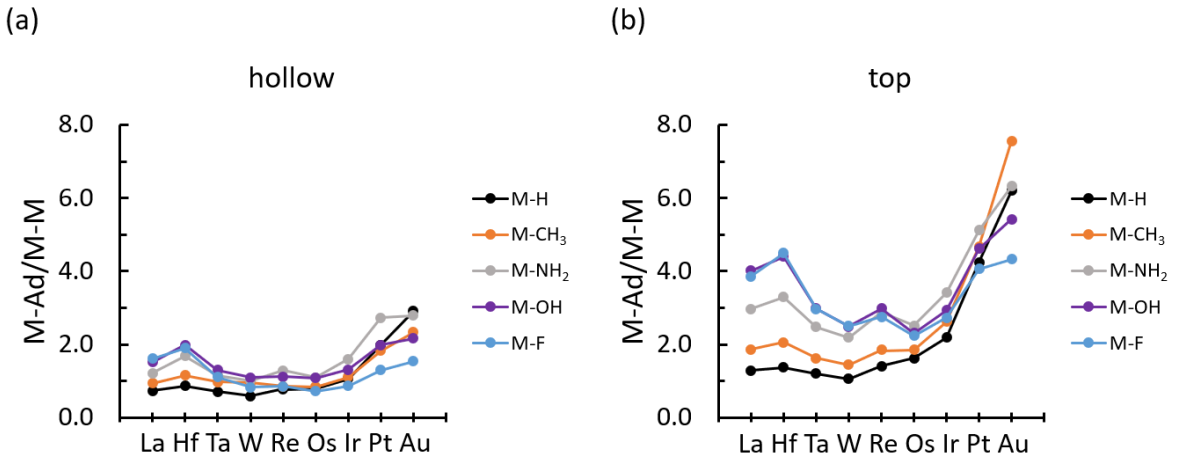

Figure 17. Average ICOHP value for the M-Ad bond divided by that for the M-M bond calculated for each metal surface structure with the adsorbate adsorbed at the (a) hollow or (b) top site.

Let us try to refine our model again, keeping in mind the observations 1) and 2) noted above. However, since we have already gained a good understanding of the effects of the difference in energy level between the metal and the adsorbate, we will not consider those effects for now. We will see the combined effects of these two factors as noted later and presented in the SI. The Hamiltonian matrices for the modified model are shown in Figure 18a. By weighting the edges corresponding to the M-Ad bonds, the difference in strength between the M-M and M-Ad bonds is represented. The difference between the M-Ad bond strength at the top site and that at the hollow site is also factored in. The energy difference curve calculated under these conditions is shown in Figure 18b.

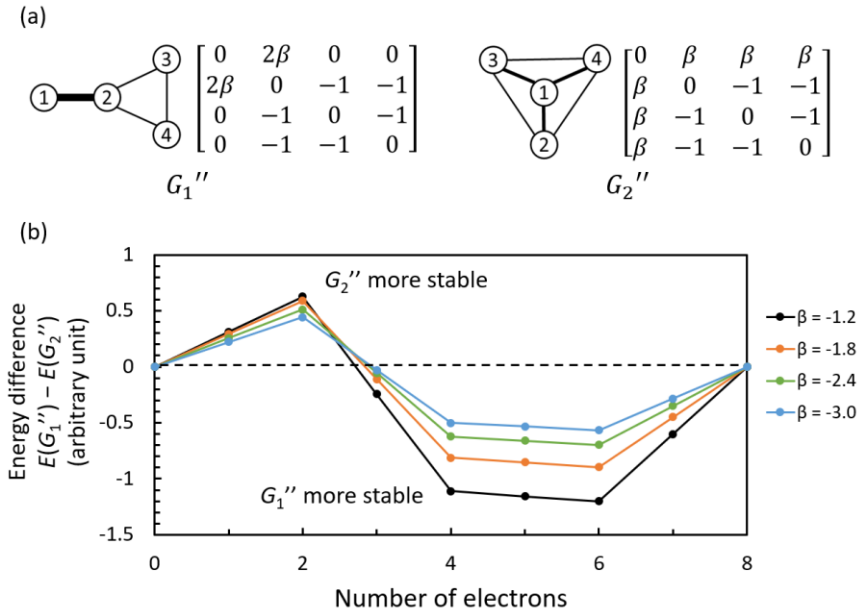

Figure 18. (a) Modified Hamiltonian matrices and corresponding graphs G_1'' and G_2''. The weighted edges, corresponding to the M-Ad bond, are represented by thicker lines. (b) The energy difference curve for G_1'' and G_2'' obtained by the method similar to that used to obtain the energy difference curve in Figure 5. Here, the value of β in the Hamiltonian matrices was varied from -1.2 to -3.0.

From Figure 18b, one can see that there is a significant change at high electron counts. As the M-Ad bond becomes stronger, the depth of the valley bottom of the energy difference curve becomes shallower. The adsorption state at the top site appears to get less stable. On the other hand, at low electron counts, the height of the hill top becomes lower and lower, but the degree to which the top gets lower is smaller than the degree to which the bottom gets higher.

As shown in Figure 15, taking the difference in the energy levels between the metal and the adsorbate into account, at high electron counts, the trend of change in the energy difference curve observed is similar to what is observed here. However, the trend observed at low electron counts is different between Figure 15 and Figure 18. It follows from this that if we

take both of the two factors into account at the same time, the change in the energy difference curve at high electron counts will be accentuated, while that will be less noticeable at low electron counts (see the SI). This suggests that the result output from our simple model is asymptotically approaching the observed fact that for many adsorbed species, the degree of stabilization of adsorption is greater at the hollow site than at the top site, as shown in Figure 7.

We have rationalized the change in the energy difference curve shown in Figure 15b based on the walks shown in Figure 16, can something similar be done here to rationalize that in Figure 18b? Now let us see how the walk of length 3 changes with the introduction of the parameter of β. On graph G_1'', there is no walk of length 3 through the weighted edge. On the other hand, on graph G_2'', there are some, as shown in Figure 19. These walks appear to be counting triangles that the adsorbate takes part in.

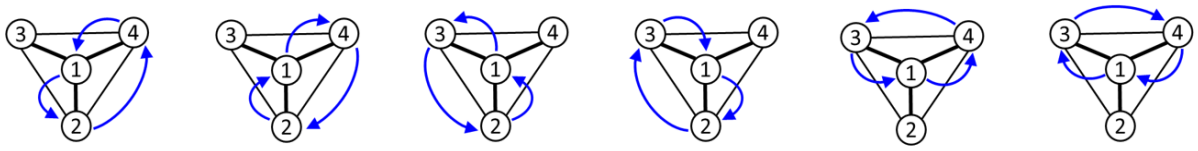

Figure 19. Walks on G_2'' which get to make an important contribution to the third moment as the parameter of β introduced. Since each walk passes through the weighted edge twice and the non-weighted edge once, the contribution of each to the third moment is $-\beta^2$.

What we witnessed above, at first glance, would help the adsorption structure at the hollow site have a more negative value of the third moment. The height of the top of the hill at low electron counts was expected to increase as the strength of the M-Ad bond increases, but

this turned out not to be true. On top of that, in the SI, the difference in μ_3 between G_1'' and G_2'' is plotted against β, and it can be seen that the difference shrinks as the absolute value of β increases. What in the world is going on here? The complexity lurking in the simplicity inspires us to explore it as detailed below.

Note that the third moment we are looking at here is the one obtained after the second moment scaling, where the nth moment is scaled by the factor of $\mu_2{}^{-n/2}$.[75] Since $\mu_2 \sim \beta^2$ (see Figure 20), the third moment is scaled by $\mu_2{}^{-3/2} \sim \beta^{-3}$. The third moment for G_2'' before scaled is of the order of β^2 (see Figure 19), so after scaled, it is of the order of β^{-1}. As for G_1', the third moment before scaled is independent of β, so after scaled, it is of the order of β^{-3}. By comparing them, one can see that the difference in the third moment between G_1'' and G_2'' is governed by β^{-1}. This may be the reason why the difference in the third moment becomes smaller as the absolute value of β increases. Given the above, what we saw in Figure 18 turned out to be a decrease in the peak amplitude of the energy difference curve, caused by the decrease in the difference in the third moment due to the second moment scaling. Nevertheless, note that the value of the third moment for G_2'' is still more negative than that for G_1'', so the shape of the curve can be said to be unchanged in a qualitative sense.

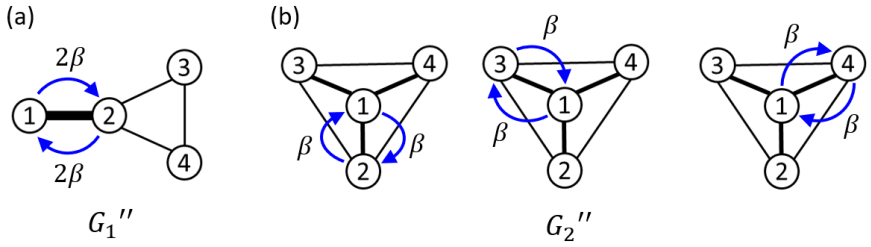

Figure 20. Walks on (a) G_1'' and (b) G_2'' which get to make an important contribution to the second moment as the parameter of β introduced. The contribution is on the order of the square of β.

We would like to note that a more detailed discussion of the intervention of the second moment in the energy difference curve dominated by the third moment can be found in the literature.[52,55] The reader may have already realized a consequence of the effect of the second moment on the energy difference curve dominated by the third moment already in this paper as well. It can be seen in the energy difference curves for the adsorption of the N and O atoms. The shape of their energy difference curves implies the dominance of the third moment, but for all of the metals, adsorption at the hollow site is preferred over at the top site. This is probably because the M-N and M-O bonds are much stronger than the M-M bonds, and the second moment for these structures would be evaluated as large.

Data supporting the above claim is presented in the SI. Graphs of the ICOHP values calculated for the M-O and M-N bonds are shown there: compared to the strength of the M-H, M-CH_3, M-NH_2, M-OH, and M-F bonds, the M-O bond is about twice as strong, and the M-N bond is about thrice as strong. On top of that, when the strength of the M-O and M-N bonds were artificially weakened on the computer, it was observed that the adsorption at the top site

becomes more stable than that at the hollow site.

Things may not be so simple. Unlike the ligands shown in Figure 1, which are in the isolobal relationship, the contribution of π-bonds cannot be ignored in the adsorption of N and O atoms (see the SI for more detail). As it stands, our simple model cannot explicitly capture such an effect. It can only be incorporated as a difference in the strength of the bond. Further improvement of the model is an issue for the future.

The attempt in this paper to understand site preference on surfaces in the context of the method of moments can also be related to the so-called coloring problem of site preference in solids and molecules, as elaborated by Burdett and co-workers.[52,113,114] An ultimately simple example of the coloring problem is the question of whether the A-B-A or A-A-B molecule is more stable. Assume that atom B has a higher electronegativity than atom A. In other words, the diagonal element of the Hamiltonian matrix corresponding to atom B is more negative than that for atom A. Thus, it can be seen that the self-returning walk on atom B is more important than that on atom A.

Figure 21a shows the typical shape of the energy difference curve for A-B-A vs. A-A-B.[52] The shape of the curve suggests that this is a third moment problem. The A-B-A molecule is more stable at low electron counts, while the A-A-B molecule more stable at high electron counts. This means that the A-B-A molecule has a more negative value of μ_3 than the A-A-B molecule. However, neither of the molecules has a triangular topology. The difference in the

coordination number around the B atom with high electronegativity creates the difference in μ_3 (see Figure 21b). This is exactly the same situation we witnessed in Figure 16. The minimum requirement for discussing the problem of site preference may be the difference in coordination number. However, we would like to add that a change in the number of triangles around an adsorption site will require a change in its coordination number. Note that this is not always true for the molecular system.

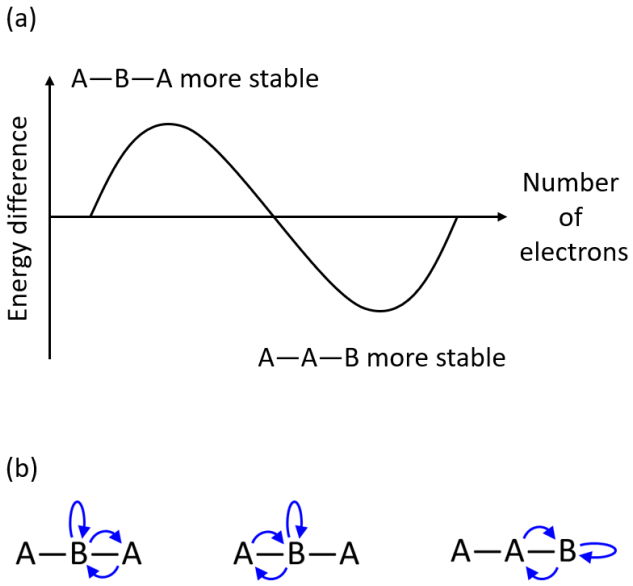

Figure 21. (a) Schematic representation of the energy difference curve for whether the ABA or AAB molecule is more stable. This figure was drawn by referring to what is found in the literature.[52] The curve suggests that this is a third moment problem. (b) Walks expected to play a decisive role in producing the difference in the third moment between the ABA and AAB molecules.

5. Conclusions

In this study, we have investigated the selectivity of adsorption sites for atoms and molecular fragments on the close-packed surface of transition metals using DFT calculations. There has been a vast accumulation of such computational studies as presented in the literature. However, the novelty of our study is that we have used the method of moments as an interpretative tool for explaining the results of the DFT calculations. We have clarified the consequences of the topology of the adsorption structure of atoms and molecular fragments at two typical adsorption sites, namely top and hollow.

In the hollow site adsorption, the geometric structure of a trigonal pyramid can be identified by focusing on the local coordination environment of the adsorbate atom. The pyramid consists of triangles forming the base and lateral faces. However, in the top site adsorption, such a triangular geometry cannot be found. The geometry of the triangle in the local structure, when reflected in a chemical graph representation, is reduced to the topology of a closed walk of length 3. The topology can be recovered as the third moment of the DOS obtained from the electronic structure calculation of the adsorption geometry. This is why the selectivity of adsorption sites is a matter of the third moment.

The most important consequence deduced from the dominance of the third moment is that at low band fillings, the topology with the more negative third moment, i.e., the hollow-site adsorption, is preferred, while at high band fillings, the topology with the less negative third

moment, i.e., top-site adsorption, is preferred. However, when the bond between the adsorbate atom and the metal surface is too strong, the second moment is likely to intervene in the dominance of the third moment. The stability will be skewed toward the topology with a larger second moment, i.e., the geometry with a large coordination number, which is the hollow-site adsorption structure.

Notes

The authors declare no competing financial interest.

Acknowledgements

We are grateful to Daniel C Fredrickson for his comments on this work. This work was supported by KAKENHI grants (numbers JP21K04996, JP22H00335, and JP22H05146) from the Japan Society for the Promotion of Science (JSPS) and the Ministry of Education, Culture, Sports, Science and Technology of Japan (MEXT) through the MEXT projects Integrated Research Consortium on Chemical Sciences, Cooperative Research Program of Network Joint Research Center for Materials and Devices and Elements Strategy Initiative to Form Core Research Center, and by JST-CREST JPMJCR15P5 and JST-Mirai JPMJMI18A2. We are grateful for a JSPS Grant-in-Aid for Scientific Research on Innovative Areas (Discrete Geometric Analysis for Materials Design, grant number JP20H04643, and Mixed Anion, grant number JP19H04700). The computations in this work were primarily performed using the computer facilities at the Research Institute for Information Technology, Kyushu University.

Supporting Information: Optimized structure for each adsorbed species on each surface, selectivity of the adsorption site for alkanethiol, average ICOHP values calculated, combined effects of the Coulomb and resonance integrals on the energy difference curve, difference in μ_3, ratio of the strength of the M-O or M-N bond to that of the M-M bond, change in adsorption site selectivity when the M-O and M-N bonds are weakened, role that π interactions play in O and N adsorption, and atomic coordinates of optimized slab unit cells.

References

(1) Hori, M.; Tsuji, Y.; Yoshizawa, K. Bonding of C_1 Fragments on Metal Nanoclusters: A Search for Methane Conversion Catalysts with Swarm Intelligence. *Phys. Chem. Chem. Phys.* **2021**, *23*, 14004-14015.

(2) Kamachi, T.; Ogata, T.; Mori, E.; Iura, K.; Okuda, N.; Nagata, M.; Yoshizawa, K. Computational Exploration of the Mechanism of the Hydrogenation Step of the Anthraquinone Process for Hydrogen Peroxide Production. *J. Phys. Chem. C* **2015**, *119*, 8748–8754.

(3) Morimoto, M.; Takatsuji, Y.; Iikubo, S.; Kawano, S.; Sakakura, T.; Haruyama, T. Experimental and Theoretical Elucidation of Electrochemical CO_2 Reduction on an Electrodeposited Cu3Sn Alloy. *J. Phys. Chem. C* **2019**, *123*, 3004–3010.

(4) Tsuji, Y.; Baba, T.; Tsurumi, N.; Murata, H.; Masago, N.; Yoshizawa, K. Theoretical Study on the Adhesion Interaction between Epoxy Resin Including Curing Agent and Plated Gold Surface. *Langmuir* **2021**, *37*, 3982-3995.

(5) Marcus, P. Surface Science Approach to Corrosion Phenomena. *Electrochim. Acta* **1998**, *43*, 109-118.

(6) Bohnen, K. P.; Kiwi, M.; Suhl, H. Friction Coefficient of an Adsorbed H Atom on a Metal Surface. *Phys. Rev. Lett.* **1975**, *34*, 1512-1515.

(7) Tsuji, Y.; Semoto, T.; Yoshizawa, K. A Bipodal Dicyano Anchor Unit for Single‐Molecule Spintronic Devices. *ChemPhysChem* **2013**, *14*, 2470-2475.

(8) Reimers, R. J.; Solomon, C. G; Gagliardi, A.; Bilic, A.; Hush, S. N.; Frauenheim, T.; Di Carlo, A.; Pecchia, A. The Green's Function Density Functional Tight-Binding (gDFTB) Method for Molecular Electronic Conduction. *J. Phys. Chem. A* **2007**, *111*, 5692-5702.

(9) Tsutsui, M.; Taniguchi, M. Single Molecule Electronics and Devices. *Sensors* **2012**, *12*, 7259–7298.

(10) Taylor, H. S.; Burns, R. M. The Adsorption of Gases by Metallic Catalysis. *J. Am. Chem. Soc.* **1921**, *43*, 1273-1287.

(11) Benton, A. F. Adsorption and Solution of Gases by Metals. *Trans. Faraday Soc.* **1932**, *28*, 202-218.

(12) Brennan, D.; Hayward, D. O.; Trapnell, B. M. W. The Calorimetric Determination of the Heats of Adsorption of Oxygen on Evaporated Metal Films. *Proc. R. Soc. London* **1960**, *A256*, 81-105.

(13) J. C. P. Mignolet, Relation between the Surface Potential and the Interaction Energy in the Case of Some Hydrogen Films. *J. Chem. Phys.* **1955**, *23*, 753.

(14) Stevenson, D. P. Heat of Chemisorption of Hydrogen in Metals. *J. Chem. Phys.* **1955**, *23*, 203.

(15) Bond, G. C. *Catalysis by Metals*; Academic Press: London and New York, 1962, p 84.

(16) Eischens, R. P.; Francis, S. A.; Pliskin, W. A. The Effect of Surface Coverage on the Spectra of Chemisorbed CO. *J. Phys. Chem.* **1956**, *60*, 194–201.

(17) Eischens, R. P.; Pliskin, W. A. The Infrared Spectra of Adsorbed Molecules. *Adv. Catal.* **1958**, 10, 1-56.

(18) Yang, A. C.; Garl, C. W. Infrared Studies of Carbon Monoxide Chemisorbed on Rhodium. *J. Phys. Chem.* **1957**, *61*, 1504-1512.

(19) Gates, J. A.; Kesmodel, L. L. Surface Vibrational Spectroscopy with Angle-Dependent Electron Energy Loss Spectroscopy: Acetylene Chemisorption on Pd (111). *J. Chem. Phys.* **1982**, *76*, 4281-4286

(20) Koel, B. E.; Somorjai, G. A. Surface Structural Chemistry. In *Catalysis, Science and Technology*, Anderson, J. R., Boudart, M., Eds.; Springer-Verlag: Berlin, 1985; Vol. 7, pp 159-218.

(21) Bent, B. E.; Mate, C. M.; Crowell, J. E.; Koel, B. E.; Somorjai, G. A. Bonding and Thermal Decomposition of Propylene, Propadiene, and Methylacetylene on the Rhodium(111) Single-Crystal Surface. *J. Phys. Chem.* **1987**, *91*, 1493-1502.

(22) Bartram, M. E.; Koel, B. E. Summary Abstract: NO_2 Chemisorption: An Example of Surface Linkage Isomerism. *J. Vac. Sci. Technol., A* **1988**, *6*, 782-783.

(23) Froitzheim, H.; Hopster, H.; Ibach, H.; Lehwald, S. Adsorption sites of CO on Pt(111). *Appl. Phys.* **1977**, *13*, 147-151.

(24) Andersson, S. Surface Vibrational Excitations of O in the p(2 × 2)O and c(2 × 2)O Structures on Ni(100). *Sol. State Comm.* **1976**, *20*, 229-232.

(25) Froitzheim, H.; Ibach, H.; Lehwald, S. Surface Vibrations of Oxygen on W(100). *Phys. Rev. B* **1976**, *14*, 1362-1369.

(26) Andersson, S. Vibrational Excitations and Structure of H_2, D_2 and HD Absorbed on Ni (100). *Chem. Phys. Lett.* **1978**, *55*, 185-188.

(27) Somorjai, G. A.; Li, Y. *Introduction to Surface Chemistry and Catalysis*, 2nd ed.; John Wiley & Sons Inc.: Hoboken, 2010.

(28) Vasić, D.; Ristanović, Z.; Pašti, I.; Mentus, S. Systematic DFT-GGA Study of Hydrogen Adsorption on Transition Metals Russ. *J. Phys. Chem. A* **2011**, *85*, 2373-2379.

(29) Kristinsdóttir, L.; Skúlason, E. A Systematic DFT Study of Hydrogen Diffusion on Transition Metal Surfaces. *Surf. Sci.* **2012**, *606*, 1400-1404.

(30) Bernard Rodríguez, C. R.; Santana, J. A. J. Adsorption and Diffusion of Sulfur on the (111), (100), (110), and (211) Surfaces of FCC Metals: Density Functional Theory Calculations. *J. Chem. Phys.* **2018**, *149*, 204701.

(31) Zeng, Z.-H.; Da Silva, J. L. F.; Li, W.-X. Theory of Nitride Oxide Adsorption on Transition Metal (111) Surfaces: A First-Principles Investigation. *Phys. Chem. Chem. Phys.* **2010**, *12*, 2459-2470.

(32) Gunasooriya, G. T. K. K.; Saeys, M. CO Adsorption Site Preference on Platinum: Charge Is the Essence. *ACS Catal.* **2018**, *8*, 3770-3774.

(33) Albright, T. A.; Burdett, J.; Whangbo, M.-H. *Orbital Interactions in Chemistry*, 2nd ed.; Wiley: Hoboken, 2013.

(34) Hoffmann, R. *Solids and Surfaces: A Chemist's View of Bonding in Extended Structures*; Wiley-VCH: Weinheim, 1988.

(35) Saillard, J. Y.; Hoffmann, R. Carbon-Hydrogen and Hydrogen-Hydrogen Activation in Transition Metal Complexes and on Surfaces. *J. Am. Chem. Soc.* **1984**, *106*, 2006-2026.

(36) Zheng, C.; Apeloig, Y.; Hoffmann, R. Bonding and Coupling of C1 Fragments on Metal Surfaces. *J. Am. Chem. Soc.* **1988**, *110*, 749-774.

(37) Papoian, G.; Nørskov, J. K.; Hoffmann, R. A Comparative Theoretical Study of the Hydrogen, Methyl, and Ethyl Chemisorption on the Pt (111) Surface. *J. Am. Chem. Soc.* **2000**, *122*, 4129-4144.

(38) Tachibana, M.; Yoshizawa, K.; Ogawa, A.; Fujimoto, H.; Hoffmann, R. Sulfur/Gold Orbital Interactions which Determine the Structure of Alkanethiolate/Au(111) Self-Assembled Monolayer Systems. *J. Phys. Chem. B* **2002**, *106*, 12727-12736.

(39) Elian, M.; Chen, M. M. L.; Mingos, D. M. P.; Hoffmann, R. Comparative Bonding Study of Conical Fragments. *Inorg. Chem.* **1976**, *15*, 1148-1155.

(40) Hoffmann, R. Building Bridges Between Inorganic and Organic Chemistry (Nobel Lecture). *Angew. Chem., Int. Ed. Engl.* **1982**, *21*, 711-724.

(41) Hall, K. P.; Mingos, D. M. P. Homo- and Heteronuclear Cluster Compounds of Gold. *Prog. Inorg. Chem.* **2007**, *32*, 237-325.

(42) Zangwill, A. *Physics at Surfaces*; Cambridge University Press: Cambridge, 1988.

(43) Dynamics. In *Handbook of Surface Science*; Hasselbrink, E., Lundqvist, B. I., Eds.; Elsevier, 2008; Vol. 3, pp 1-1015.

(44) Bauer, E. *Surface Microscopy with Low Energy Electrons*; Springer: New York, 2014.

(45) Kolasinki, K. W. *Surface Science*, 2nd ed.; Wiley: New York, 2008.

(46) Paul, J.-F.; Sautet, P. Density-Functional Periodic Study of the Adsorption of Hydrogen on a Palladium (111) Surface. *Phys. Rev. B* **1996**, *53*, 8015.

(47) Vargas, M. C.; Giannozzi, P.; Selloni, A.; Scoles, G. Coverage-Dependent Adsorption of CH_3S and $(CH_3S)_2$ on Au(111): A Density Functional Theory Study. *J. Phys. Chem. B* **2001**, *105*, 9509-9513.

(48) Løvvik, O. M.; Olsen, R. A. Adsorption Energies and Ordered Structures of Hydrogen on Pd(111) from Density-Functional Periodic Calculations. *Phys. Rev. B* **1998**, *58*, 10890-10898.

(49) Kuwabara, A.; Saito, Y.; Koyama, Y.; Oba, F.; Matsunaga, K.; Tanaka, I. First Principles Calculation of CO and H_2 Adsorption on Strained Pt Surface. *Mater. Trans.* **2008**, *49*, 2484-2490.

(50) Cyrot-Lackmann, F. On the Electronic Structure of Liquid Transitional Metals. *Adv. Phys.* **1967**, *16*, 393-400.

(51) Ducastelle, F.; Cyrot-Lackmann, F. Moments Developments: II. Application to the Crystalline Structures and the Stacking Fault Energies of Transition Metals. *J. Phys. Chem. Solids* **1971**, *32*, 285-301.

(52) Burdett, J. K. Some Structural Problems Examined Using the Method of Moments. *Struct. Bonding (Berlin)* **1987**, *65*, 29−90.

(53) Burdett, J. K. *Chemical Bonds: A Dialogue*; Wiley: New York, 1997.

(54) Burdett, J. K. *Chemical Bonding in Solids*; Oxford University Press: New York, 1995.

(55) Burdett, J. K.; Lee, S. Moments and the Energies of Solids. *J. Am. Chem. Soc.* **1985**, *107*, 3050-3063.

(56) Lee, S. Structural Diversity in Solid State Chemistry: A Story of Squares and Triangles. *Annu. Rev. Phys. Chem.* **1996**, *47*, 397-419.

(57) Lee, S. Second-Moment Scaling and Covalent Crystal Structures. *Acc. Chem. Res.* **1991**, *24*, 249-254.

(58) Shah, M.; Pettifor, D. G. Structural Stability, Local Topology and Electron Count in

Small s-Valent Clusters. *J. Alloys Compd.* **1993**, *197*, 145-152.

(59) Pettifor, D. G. *Bonding and Structure of Molecules and Solids*; Clarendon Press; Oxford University Press: Oxford: New York, 1995.

(60) Johnston, R. L.; Hoffmann, R. The Kagomé Net: Band Theoretical and Topological Aspects. *Polyhedron* **1990**, *9*, 1901-1911.

(61) Stacey, T. E.; Fredrickson, D. C. Perceiving Molecular Themes in the Structures and Bonding of Intermetallic Phases: The Role of Hückel Theory in an Ab Initio Era. *Dalton Trans.* **2012**, *41*, 7801-7813.

(62) Stacey, T. E.; Fredrickson, D. C. The μ_3 Model of Acids and Bases: Extending the Lewis Theory to Intermetallics. *Inorg. Chem.* **2012**, *51*, 4250-4264.

(63) Stacey, T. E.; Fredrickson, D. C. Structural Acid-Base Chemistry in the Metallic State: How μ_3-Neutralization Drives Interfaces and Helices in $Ti_{21}Mn_{25}$. *Inorg. Chem.* **2013**, *52*, 8349-8359.

(64) Frederickson, D. C. Electronic Packing Frustration in Complex Intermetallic Structures: The Role of Chemical Pressure in Ca_2Ag_7. *J. Am. Chem. Soc.* **2011**, *133*, 10070-10073.

(65) Cyrot-Lackmann, F. On the Calculation of Surface Tension in Transition Metals. *Surf. Sci.* **1969**, *15*, 535-548.

(66) Desjonqueres, M. C.; Cyrot-Lackmann, F. On the Local Densities of States on Flat and Stepped Pt Surfaces. *Solid State Commun.* **1976**, *18*, 1127-1132.

(67) Haydock, R.; Kelly, M. J. Surface Densities of States in Tight-Binding Approximations. *Surf. Sci.* **1973**, *38*, 139-148.

(68) Desjonqueres, M. C.; Cyrot-Lackmann, F. Surface Densities of States in Cleaved Transition Metals. *J. Phys. F* **1975**, *5*, 1368-1384.

(69) Lambin, P.; Gaspard, J. P. Analysis of the Density of States of Binary Alloys. II. Surface Segregation. *J. Phys. F* **1980**, *10*, 2413-2428.

(70) Trinajstić, N. *Chemical Graph Theory*; CRC Press: Boca Raton, 1992.

(71) Tsuji, Y.; Estrada, E.; Movassagh, R.; Hoffmann, R. Quantum Interference, Graphs, Walks, and Polynomials. *Chem. Rev.* **2018**, *118*, 4887-4911.

(72) Tsuji, Y.; Yoshizawa, K. From Infection Clusters to Metal Clusters: Significance of the Lowest Occupied Molecular Orbital (LOMO). *ACS Omega* **2021**, *6*, 1339-1351.

(73) Heilbronner, E.; Bock, H. *The HMO-Model and Its Applications, Basis and Manipulation*; J. Wiley & Sons: London, 1976.

(74) Pettifor, D. G. The Structures of Binary Compounds. I. Phenomenological Structure Maps. *J. Phys. C: Solid State Phys.* **1986**, *19*, 285-313.

(75) Clark, P. M.; Lee, S.; Fredrickson, D. C. Transition Metal AB_3 Intermetallics: Structure Maps Based on Quantum Mechanical Stability. *J. Solid State Chem.* **2005**, *178*, 1269-1283.

(76) Kresse, G.; Hafner, J. Ab Initio Molecular Dynamics for Liquid Metals. *Phys. Rev. B* **1993**, *47*, 558-561.

(77) Kresse, G.; Hafner, J. Ab Initio Molecular-Dynamics Simulation of the Liquid-Metal-Amorphous-Semiconductor Transition in Germanium. *Phys. Rev. B* **1994**, *49*, 14251-14269.

(78) Kresse, G.; Furthmüller, J. Efficiency of Ab-Initio Total Energy Calculations for Metals and Semiconductors Using a Plane-Wave Basis Set. *Comput. Mater. Sci.* **1996**, *6*, 15-50.

(79) Kresse, G.; Furthmüller, J. Efficient Iterative Schemes for Ab Initio Total-Energy Calculations Using a Plane-Wave Basis Set. *Phys. Rev. B* **1996**, *54*, 11169-11186.

(80) Heimel, G.; Romaner, L.; Bredas, J. L.; Zojer, E. Odd−Even Effects in Self-Assembled Monolayers of ω-(Biphenyl-4-yl) alkanethiols: A First-Principles Study. *Langmuir* **2008**, *24*, 474-482.

(81) Vericat, C.; Vela, M. E.; Salvarezza, R. C. Self-Assembled Monolayers of Alkanethiols on Au(111): Surface Structures, Defects and Dynamics. *Phys. Chem. Chem. Phys.* **2005**, *7*, 3258–3268.

(82) Perdew, J. P.; Burke, K.; Ernzerhof, M. Generalized Gradient Approximation Made Simple. *Phys. Rev. Lett.* **1996**, *77*, 3865-3868.

(83) Blöchl, P. E. Projector Augmented-Wave Method. *Phys. Rev. B* **1994**, *50*, 17953-17979.

(84) Kresse, G.; Joubert, D. From Ultrasoft Pseudopotentials to the Projector Augmented-Wave Method. *Phys. Rev. B* **1999**, *59*, 1758-1775.

(85) Grimme, S.; Ehrlich, S.; Goerigk, L. Effect of the Damping Function in Dispersion Corrected Density Functional Theory. *J. Comput. Chem.* **2011**, *32*, 1456-1465.

(86) Tsuji, Y.; Kitamura, Y.; Someya, M.; Takano, T.; Yaginuma, M.; Nakanishi, K.; Yoshizawa, K. Adhesion of Epoxy Resin with Hexagonal Boron Nitride and Graphite. *ACS Omega* **2019**, *4*, 4491-4504.

(87) Momma, K.; Izumi, F. VESTA 3 for Three-Dimensional Visualization of Crystal, Volumetric and Morphology Data. *J. Appl. Crystallogr.* **2011**, *44*, 1272-1276.

(88) Dronskowski, R.; Bloechl, P. E. Crystal Orbital Hamilton Populations (COHP): Energy-Resolved Visualization of Chemical Bonding in Solids Based on Density-Functional Calculations. *J. Phys. Chem.* **1993**, *97*, 8617-8624.

(89) Rohling, R. Y.; Tranca, I. C.; Hensen, E. J. M.; Pidko, E. A. Correlations between Density-Based Bond Orders and Orbital-Based Bond Energies for Chemical Bonding Analysis. *J. Phys. Chem. C* **2019**, *123*, 2843-2854.

(90) Deringer, V. L.; Tchougreeff, A. L.; Dronskowski, R. Crystal Orbital Hamilton Population (COHP) Analysis as Projected from Plane-Wave Basis Sets. *J. Phys. Chem. A* **2011**, *115*, 5461-5466.

(91) Maintz, S.; Deringer, V. L.; Tchougréeff, A. L.; Dronskowski, R. Analytic Projection from Plane-Wave and PAW Wavefunctions and Application to Chemical-Bonding Analysis in Solids. *J. Comput. Chem.* **2013**, *34*, 2557-2567.

(92) Maintz, S.; Deringer, V. L.; Tchougréeff, A. L.; Dronskowski, R. LOBSTER: A Tool to Extract Chemical Bonding from Plane-Wave Based DFT. *J. Comput. Chem.* **2016**, *37*, 1030-1035.

(93) Görne, A. L.; Dronskowski, R. Covalent Bonding Versus Total Energy: On the Attainability of Certain Predicted Low-Energy Carbon Allotropes. *Carbon* **2019**, *148*, 151-158.

(94) Aditya, I. D.; Matsunaka, D.; Shibutani, Y.; Suprijadi. Interfacial Interaction between Carbon Nanotube and Stoichio- and Nonstoichiometric Ceramic Surfaces by Ab-Initio Calculations. *Mater. Trans.* **2018**, *59*, 1684-1690.

(95) Hoffmann, R. An Extended Hückel Theory. I. Hydrocarbons. *J. Chem. Phys.* **1963**, *39*, 1397-1412.

(96) Stokbro, K.; Petersen, D. E.; Smidstrup, S.; Blom, A.; Ipsen, M.; Kaasbjerg, K. Semiempirical Model for Nanoscale Device Simulations. *Phys. Rev. B* **2010**, *82*, 075420

(97) *Atomistix ToolKit*, version 2019; QuantumWise A/S, 2019.

(98) Landrum, G. A.; Glassey, W. V. *YAeHMOP: Yet Another extended Huckel Molecular Orbital Package*, version 3.0, **2018**. http://yaehmop.sourceforge.net/ (accessed Dec 13, 2021)

(99) Avery, P.; Ludowieg, H.; Autschbach, J.; Zurek, E. Extended Hückel Calculations on Solids Using the Avogadro Molecular Editor and Visualizer. *J. Chem. Educ.* **2018**, *95*, 331–337.

(100) Alvarez, S. *Table of Parameters for Extended Hückel Calculations*; Universitat de Barcelona: Barcelona, 1993.

(101) Hoffmann, R.; Alvarez, S.; Mealli, C.; Falceto, A.; Cahill, T. J., III; Zeng, T.; Manca, G. From Widely Accepted Concepts in Coordination Chemistry to Inverted Ligand Fields. *Chem. Rev.* **2016**, *116*, 8173-8192.

(102) Friedel, J. Metallic Alloys. *Nuovo Cimento* **1958**, *7*, 287-311.

(103) Gómez-Jeria, S. J. The Limits of the Extended Hückel Theory to Calculate the Total Density of States of Medium-Sized Molecules. *J. Chil. Chem. Soc.* **2006**, *51*, 1061-1064.

(104) Mann, J. B.; Meek, T. L.; Knight, E. T.; Capitani, J. F.; Allen, L. C. Configuration Energies of the d-Block Elements. *J. Am. Chem. Soc.* **2000**, *122*, 5132-5137.

(105) Schilling, B. E. R.; Hoffmann, R. M_3L_9(Ligand) Complexes. *J. Am. Chem. Soc.* **1979**,

101, 3456-3467.

(106) Silvestre, J.; Hoffmann, R. C_2H_n Fragments on Metal Surfaces. *Langmuir* **1985**, *1*, 621-647.

(107) Ertural, C.; Steinberg, S.; Dronskowski, R. Development of a Robust Tool to Extract Mulliken and Löwdin Charges from Plane Waves and Its Application to Solid-State Materials. *RSC Adv.* **2019**, *9*, 29821-29830.

(108) Nelson, R.; Ertural, C.; George, J.; Deringer, V. L.; Hautier, G.; Dronskowski, R. LOBSTER : Local Orbital Projections, Atomic Charges, and Chemical-Bonding Analysis from Projector-Augmented-Wave-Based Density-Functional Theory. *J. Comput. Chem.* **2020**, *41*, 1931-1940.

(109) Rahm, M.; Zeng, T.; Hoffmann, R. Electronegativity Seen as the Ground-State Average Valence Electron Binding Energy. *J. Am. Chem. Soc.* **2019**, *141*, 342-351.

(110) Jolly, W. L.; Perry, W. B. Calculation of Atomic Charges by an Electronegativity Equalization Procedure. *Inorg. Chem.* **1974**, *13*, 2686-2692.

(111) Little, E. J., Jr.; Jones, M. M. A Complete Table of Electronegativities. *J. Chem. Educ.* **1960**, *37*, 231-233.

(112) Economou, E. *The Physics of Solids, Essentials and Beyond*; Springer: Heidelberg, 2010.

(113) Burdett, J. K.; Lee, S.; McLarnan, T. J. Coloring Problem. *J. Am. Chem. Soc.* **1985**, *107*, 3083-3089.

(114) Burdett, J. K. Why Are the Structures of Some Solids So Complex but Others So Simple? *Inorg. Chem.* **1994**, *33*, 1848-1856.

TOC Graphic